Supplementary Information for
Exacerbated drought impacts on global ecosystems due to structural overshoot

Yao Zhang[1,2,3]*, Trevor F. Keenan[1,2]*, Sha Zhou[1,2,4,5]

[1]Climate and Ecosystem Sciences Division, Lawrence Berkeley National Laboratory, Berkeley, CA, USA

[2]Department of Environmental Science, Policy and Management, UC Berkeley, Berkeley, CA, USA

[3]Sino-French Institute for Earth System Science, College of Urban and Environmental Sciences, Peking University, Beijing, China

[4]Department of Earth and Environmental Engineering, Columbia University, New York, NY, USA

[5]State Key Laboratory of Earth Surface Processes and Resources Ecology, Faculty of Geographical Science, Beijing Normal University, Beijing, China

*Corresponding author: zhangyao@pku.edu.cn; trevorkeenan@berkeley.edu

The SI contains 5 Supplementary Text, 1 Supplementary Table, 19 Supplementary Figures, and Supplementary References.

Supplementary Text 1. Bayes forward filtering for estimating DLM coefficients.

We use the DLM to obtain the dynamic sensitivities of NDVI to previous months' NDVI and precipitation. the DLM consists of two equations: one observation equation and one state evolution equation:

$$y_t = F_t^T \boldsymbol{\theta}_t + v_t \tag{1a}$$

$$\boldsymbol{\theta}_t = G\boldsymbol{\theta}_{t-1} + W_t \tag{1b}$$

The model decomposes the time series of NDVI observations (y_t) into three components, i.e., the local/trend component (subscript l), the seasonal component (subscript s), and the regression component (subscript r). Similarly, the regressor vector (F_t), the state vector ($\boldsymbol{\theta}_t$), and the state evolution matrix (G) also consist of three corresponding components.

$$F_t = \begin{bmatrix} F_l \\ F_s \\ F_{r,t} \end{bmatrix}, \boldsymbol{\theta}_t = \begin{bmatrix} \boldsymbol{\theta}_{l,t} \\ \boldsymbol{\theta}_{s,t} \\ \boldsymbol{\theta}_{r,t} \end{bmatrix}, G = \begin{bmatrix} G_l & 0 & 0 \\ 0 & G_s & 0 \\ 0 & 0 & G_r \end{bmatrix} \tag{2}$$

(1) The local component describes the mean and trend of the NDVI, with

$$F_l = \begin{bmatrix} 1 \\ 0 \end{bmatrix}, \boldsymbol{\theta}_{l,t} = \begin{bmatrix} \theta_{l1,t} \\ \theta_{l2,t} \end{bmatrix}, G_l = \begin{bmatrix} 1 & 1 \\ 0 & 1 \end{bmatrix}$$

where $\theta_{l1,t}$ and $\theta_{l2,t}$ indicate the mean and trend at time step t, respectively. With these, Eq. (1a) and Eq. (1b) can be rewritten as:

$$y_{l,t} = \begin{bmatrix} 1 \\ 0 \end{bmatrix}^T \begin{bmatrix} \theta_{l1,t} \\ \theta_{l2,t} \end{bmatrix} + v_{l,t} = \theta_{l1,t} + v_{l,t} \tag{3a}$$

$$\boldsymbol{\theta}_{l,t} = \begin{bmatrix} \theta_{l1,t} \\ \theta_{l2,t} \end{bmatrix} = \begin{bmatrix} 1 & 1 \\ 0 & 1 \end{bmatrix} \begin{bmatrix} \theta_{l1,t-1} \\ \theta_{l2,t-1} \end{bmatrix} + w_{l,t} = \begin{bmatrix} \theta_{l1,t-1} + \theta_{l2,t-1} \\ \theta_{l2,t-1} \end{bmatrix} + w_{l,t} \tag{3b}$$

(2) The seasonal component is a combination of three Fourier forms of seasonality with frequencies at $\omega_1 = \frac{\pi}{6}$, $\omega_2 = \frac{\pi}{3}$, and $\omega_3 = \frac{2\pi}{3}$,

$$F_s = \begin{bmatrix} F_{s1} \\ F_{s2} \\ F_{s3} \end{bmatrix}, \boldsymbol{\theta}_{s,t} = \begin{bmatrix} \boldsymbol{\theta}_{s1,t} \\ \boldsymbol{\theta}_{s2,t} \\ \boldsymbol{\theta}_{s3,t} \end{bmatrix}, G_s = \begin{bmatrix} G_{s1} & 0 & 0 \\ 0 & G_{s2} & 0 \\ 0 & 0 & G_{s3} \end{bmatrix}$$

where

$$F_{s(i)} = \begin{bmatrix} 1 \\ 0 \end{bmatrix}, \boldsymbol{\theta}_{s(i),t} = \begin{bmatrix} \theta_{s(i),1,t} \\ \theta_{s(i),2,t} \end{bmatrix}, G_{s(i)} = \begin{bmatrix} \cos \omega_i & \sin \omega_i \\ -\sin \omega_i & \cos \omega_i \end{bmatrix}, \quad i \in \{1,2,3\}$$

With the historical data before time step t, the expectation of the seasonal component at time $t + k$ can be expressed as the summation of three cosines functions with different frequency, amplitude and phases:

$$\mathbb{E}[y_{s,t+k}|y_{s,1}, \ldots, y_{s,t}] = F_s^T \boldsymbol{\theta}_{s,t+k}$$

$$= \sum_{i=1}^{3} F_{s(i)}^T G_{s(i)}{}^k \boldsymbol{\theta}_{s(i),t}$$

$$= \sum_{i=1}^{3} [1 \quad 0] \begin{bmatrix} \cos \omega_i k & \sin \omega_i k \\ -\sin \omega_i k & \cos \omega_i k \end{bmatrix} \begin{bmatrix} \theta_{s(i),1,t} \\ \theta_{s(i),2,t} \end{bmatrix}$$

$$= \sum_{i=1}^{3} A_{i,t} \cos(\omega_i k + \phi_{i,t}) \qquad (4)$$

where $A_{i,t}$ and $\phi_{i,t}$ represent the magnitudes and phases of the harmonic components, respectively. Both $A_{i,t}$ and $\phi_{i,t}$ are determined by $\boldsymbol{\theta}_{s(i),t}$.

(3) The regression component uses a series of independent variables $(x_1, x_2, \ldots, x_p)$ to predict their effect on y_t.

$$F_{r,t} = [x_{1,t}, x_{2,t}, \ldots, x_{p,t}]^T, G_r = I_p$$

where I_p is the identity matrix with a dimension of p. These independent variables include the de-seasonalized detrended NDVI anomalies at different previous time scales, as well as the temperature anomalies for current month $[t]$, and precipitation anomalies from the previous 2 months to the current month $[t - 2, t]$. The de-seasonalized detrended NDVI anomalies are obtained by running the DLM for one time without the regression component, through which the trend and seasonal signal of the NDVI time series can be obtained and removed. The summation of NDVI anomalies is calculated for $[t - 3, t - 2]$ months (sub-seasonal), $[t - 6, t - 4]$ months (seasonal), $[t - 12, t - 7]$ months (intra-annual), and $[t - 24, t - 13]$ months (inter-annual). In addition, we add the previous month NDVI (lag-1) as another independent variable. In total, 7 independent variables ($p = 7$) were used (four NDVI anomalies from previous periods as the lagged effect, one NDVI anomaly from previous month as the direct effect, one temperature anomaly for temperature stress and one precipitation anomaly as the direct water stress). We did not include longer time periods since their effect on current vegetation is expected to be small.

$\boldsymbol{\theta}_{r,t}$, and the contribution from each independent variable ($y_{r,i,t} = x_{i,t}\theta_{r,i,t}$) are used for overshoot identification.

To solve the above mentioned DLM, we used a method called forward filtering. The basic idea behind this method is similar to Kalman Filtering, with an additional step to back propagate the posterior estimate of y_t to get the posterior estimate of $\boldsymbol{\theta}_t$. To do this, we first assume that the variance of noise v_t and $\boldsymbol{W}_t$ are known.

(a) Posterior at $t-1$. Given all observations $D_{t-1} = \{y_1, y_2, ..., y_{t-1}\}$, $\boldsymbol{\theta}_{t-1}$ is assumed to follow a multivariate normal distribution:

$$\boldsymbol{\theta}_{t-1}|D_{t-1} \sim N(\boldsymbol{m}_{t-1}, \boldsymbol{C}_{t-1}) \tag{5}$$

where $\boldsymbol{m}_{t-1}$ is the predicted mean, and $\boldsymbol{C}_{t-1}$ is the variance matrix.

(b) Prior at t. Together with Eq. (2), we can get the prior distribution of $\boldsymbol{\theta}_t$,

$$\boldsymbol{\theta}_t|D_{t-1} \sim N(\boldsymbol{a}_t, \boldsymbol{R}_t) \tag{6}$$

where

$$\boldsymbol{a}_t = \boldsymbol{G}_t\boldsymbol{m}_{t-1}, \boldsymbol{R}_t = \boldsymbol{G}_t\boldsymbol{C}_{t-1}\boldsymbol{G}_t^T + \boldsymbol{W}_t$$

(c) One step forecast. Together with Eq. (1), the predictive distribution of y_t is

$$y_t|D_{t-1} \sim N(f_t, q_t) \tag{7}$$

where

$$f_t = \boldsymbol{F}_t^T\boldsymbol{a}_t, q_t = \boldsymbol{F}_t^T\boldsymbol{R}_t\boldsymbol{F}_t + v_t$$

(d) Posterior at t. Comparing with the observed y_t and, the posterior estimation of $\boldsymbol{\theta}_t$ based all observation until time t is given by the Bayes rule:

$$p(\boldsymbol{\theta}_t|D_t) = p(\boldsymbol{\theta}_t|y_t, D_{t-1}) \propto p(\boldsymbol{\theta}_t|y_t, D_{t-1})p(y_t|\boldsymbol{\theta}_t, D_{t-1}) = N(\boldsymbol{m}_t, \boldsymbol{C}_t) \tag{8}$$

with

$$\boldsymbol{m}_t = \boldsymbol{a}_t + \boldsymbol{A}_t e_t, \boldsymbol{C}_t = \boldsymbol{R}_t - q_t\boldsymbol{A}_t\boldsymbol{A}_t^T$$

where

$$e_t = y_t - f_t, \boldsymbol{A}_t = \boldsymbol{R}_t\boldsymbol{F}_t/q_t$$

Here, $\boldsymbol{A}_t$ is the matrix of adaptive coefficients, e_t represents the one-step forecast errors. When y_t is missing due to cloud or snow, the prior from historical data $p(\boldsymbol{\theta}_t|D_{t-1})$ from Eq. (5) is used to estimate $\boldsymbol{\theta}_t$.

In practice, the variance of noise v and $\boldsymbol{W}_t$ are unknown. We therefore revised the above process for variance learning. We first assume $v_t \sim N(0, v)$ and $\boldsymbol{w}_t \sim N(0, v\,\boldsymbol{W}_t^*)$. Both v and $\boldsymbol{W}_t^*$ are unknown, and $\boldsymbol{W}_t^*$ is rescaled from $\boldsymbol{W}_t$. Conditioned on v, Eq. (5-8) share the same format,

$$\boldsymbol{\theta}_{t-1}|D_{t-1}, v \sim N(\boldsymbol{m}_{t-1}, v\,\boldsymbol{C}_{t-1}^*) \tag{9}$$

$$\boldsymbol{\theta}_t|D_{t-1}, v \sim N(\boldsymbol{a}_t, v\,\boldsymbol{R}_t^*) \tag{10}$$

$$y_t|D_{t-1}, v \sim N(f_t, v\,q_t^*) \tag{11}$$

$$\boldsymbol{\theta}_t|D_t, v \sim N(\boldsymbol{m}_t, v\,\boldsymbol{C}_t^*) \tag{12}$$

We assume the variation of observational error (v) follows an inverse-gamma (IG) distribution,

$$v|D_{t-1} \sim IG(n_{t-1}/2, d_{t-1}/2) \tag{13}$$

$$v|D_t \sim IG(n_t/2, d_t/2) \tag{14}$$

$$n_t = n_{t-1} + 1$$

$$d_t = d_{t-1} + e_t^2/q_t^*$$

where n_t is the degree of freedom, and

$$\boldsymbol{\theta}_{t-1}|D_{t-1} \sim T(\boldsymbol{m}_{t-1}, s_{t-1}\boldsymbol{C}_{t-1}^*) \tag{15}$$

$$\boldsymbol{\theta}_t|D_{t-1} \sim T(\boldsymbol{a}_t, s_{t-1}\boldsymbol{R}_t^*) \tag{16}$$

$$y_t|D_{t-1} \sim T(f_t, s_{t-1}q_t^*) \tag{17}$$

$$\boldsymbol{\theta}_t|D_t \sim T(\boldsymbol{m}_t, s_t\boldsymbol{C}_t^*) \tag{18}$$

$$s_{t-1} = d_{t-1}/n_t$$

$$s_t = d_t/n_t$$

We estimate $\boldsymbol{W}_t$ using the method of discounting. From Eq. (6), we can get the prior variance of $\boldsymbol{\theta}_t$ as $Var(\boldsymbol{\theta}_t| = D_{t-1}) = \boldsymbol{R}_t = \boldsymbol{G}_t\boldsymbol{C}_{t-1}\boldsymbol{G}_t^T + \boldsymbol{W}_t = \boldsymbol{P}_t + \boldsymbol{W}_t$, where $\boldsymbol{P}_t$ is the variance without stochastic noise, that is, $\boldsymbol{W}_t = 0$. If $\boldsymbol{W}_t \neq 0$, we can assume that $\boldsymbol{R}_t = \boldsymbol{P}_t/\delta$ with the parameter $\delta \in (0,1]$. This means that due to the stochastic noise, the variance inflates by $1/\delta - 1$ for each step, i.e., discounting the degree of freedom from n_t to δn_t (ref.[1]). The smaller δ, the larger changes in $\boldsymbol{\theta}_t$ and vice versa. To obtain relatively stable local trend and seasonal components without being affected by the anomalies, we use two different δ values, 0.999 for trend and seasonal, and 0.98 for regression components, respectively. This also allows us to have a relatively larger degree of freedom for regression, so that the NDVI anomalies can be correctly attributed to environmental influences and previous vegetation status. We initiate the model using non-informative priors of $\boldsymbol{m}_0 = \boldsymbol{0}$, $\boldsymbol{C}_0 = \boldsymbol{I}$, $n_0 = p$, $d_0 = 0.2^2 n_0$ at time step 0, allowing $\boldsymbol{\theta}_t$ to vary freely in the beginning and gradually converge with more observations. To minimize the

influence of this initial large fluctuation on overshoot identification, we recycle the first 5 years of NDVI and precipitation data (1981/7~1986/6) twice (a total of 10 years) as a "spin-up" period. We also test different lengths of "spin-up" period. The results are very similar if the "spin-up" period is longer than around 60 months. Using the randomized experiment, we also demonstrate that it has a very limited effect on overshoot trend analysis. The posterior distribution of $\boldsymbol{\theta}_t$ and other state-vector/matrices can be obtained from Eq. (16) and were saved for overshoot identification.

Supplementary Text 2. Sensitivity analysis of drought and overshoot drought identification

We set up seven different experiments to understand the sensitivities in the drought and overshoot drought identification. These seven experiments differ in DLM model structure and the parameters or thresholds used for drought or overshoot identification (Supplementary Table 1). The resultant overshoot patterns are shown in Supplementary Figs. 5-11.

The "reduced model" does not include temperature as the climate driver in the DLM, in contrast to the original model (Extended data Fig. 1). This leads to very similar drought patterns, while the lower overshoot drought number increases in higher latitudes and decreases in lower latitudes. The "extended model" uses radiation in addition to precipitation and temperature in the DLM. The resulting overshoot drought patterns are also similar to the original model. The "discrete precipitation model" is similar to the "extended model" that considers all three climate variables, but instead of using the 3-month average precipitation, it uses the precipitation from currently month, previous 1 month and previous 2 month separately in the DLM.

Experiment 1 and 2 use relaxed drought identification algorithms, with Experiment 1 allowing shorter drought lengths, and Experiment 2 allowing drought events with weaker impacts on vegetation (Supplementary Table 1). Experiment 1 shows an increase (21%) in drought numbers, and the increase for Experiment 2 is large (92%). This suggests that our current algorithm is conservative, and mainly focuses on the drought events with relatively larger impact. The number of overshoot drought, however, has relatively smaller increases (20% for Experiment 1 and 44% for Experiment 2).

Experiment 3 uses a stricter drought identification threshold, which leads to a reduction of the drought numbers by 37% and a reduction of overshoot events by 35%. The Experiment 4 uses a relaxed threshold for overshoot component identification. In Experiment 3, the lagged adverse

effect between past positive NDVI anomalies and current NDVI anomalies are less negative (P=0.25). This leads to a 52% increase in overshoot drought numbers.

Although these different experiments yield differences in the number of droughts and number of overshoot droughts. The spatial patterns of these drought occurrences are very similar to our original method (correlation coefficient ranges from 0.83 to 1 for drought and 0.65 to 0.94 for overshoot drought). The differences in these numbers mostly reflect the severity of drought and overshoot drought. We also find that our major findings (large temperature differences, faster drought development and stronger impact) still hold under these experiments.

Supplementary Text 3. Randomized experiments

We use the randomized experiments to test the effectiveness of using the DLM to capture the lagged effect of past NDVI anomalies on current NDVI. For the known overshoot drought event that happened in the central US in 2012, we have demonstrated how DLM can help identify this overshoot drought event in Extended Data Fig. 2. We know that the 2012 drought is in part due to the warm spring that stimulate vegetation growth during March to May[2]. This positive anomaly in vegetation contribute to the decline of NDVI during the drought period in June, July and August. Using the DLM, we also see a negative contribution from the previous 2-3 months during the drought period (Extended data Fig. 2i). For the randomized DLM with a group size of two (see Methods), the most severe drought periods (July/August 2012) are swapped to July/August 1989, following May/June of 2007. This random swap breaks up the linkage between the NDVI anomalies in the past and current, therefore, it is no longer considered an overshoot drought event (Supplementary Fig. 14).

At the regional scale, we identify almost no overshoot drought events in the randomized experiment with a group size of two months (Supplementary Fig. 15b), while the number of drought events do not change much. This is because droughts are identified based on concurrent NDVI, SPEI and climate anomalies, which are swapped together in the randomized experiment. If we use a larger group size, for example, 6 months, the lagged responses at sub-seasonal scale may be partially kept. The results confirm our assumption, with the patterns similar to that at sub-seasonal scale (Extended Data Fig. 3). Using the window size of 24 months, most lagged effects at the sub-seasonal, seasonal, and intra-annual scale may be retained, and the number of overshoot patterns is more like what we obtained without randomization (Fig. 1b).

However, we still see lower numbers of overshoot droughts in the randomized experiments, as compared to Fig. 1. This may be due to: 1) drought events or the lagged responses are separated by the random swap; 2) the propagation of sudden changes in DLM sensitivity (coefficients) at break points (where two swapped groups connect with each other), leading to inconsistent overshoot identification in each randomized run. This will also cause a decrease in model performance, especially for those with short group sizes (Supplementary Fig. 16).

Supplementary Text 4. Synthetic data experiment

To demonstrate the effectiveness of using the DLM to capture overshoot drought, we use synthetic data from different scenarios to test the model performance. The synthetic data is generated from a simple model that considers both environmental stress and vegetation dynamics.

$$NDVI_t = NDVI_{msc,t} + \delta NDVI_t \tag{19}$$

$$\delta NDVI_t = \varphi \delta NDVI_{t-1} + \zeta NDVI_t \tag{20}$$

$$\zeta NDVI = m \times \left(\min\big(f(T), f(SM)\big) \frac{NDVI_{msc,t-1} + \delta NDVI_{t-1}}{NDVI_{msc,t-1}} - \min\big(f(\bar{T}), f(\overline{SM})\big) \right) \tag{21}$$

NDVI for time t is considered as the summation of mean seasonal cycle (MSC) and anomaly (Eq. (19)); the anomaly term considers the legacy effect from previous month ($\varphi \delta NDVI_{t-1}$) and responses to the environment ($\zeta NDVI_t$); Eq. (21) indicates that the environmental response component is conditioned by the environmental limitation of the current month to multiyear average conditions, as well as the NDVI anomaly of the previous month. The coefficient m determines the sensitivity of NDVI to the environment.

The temperature responses in this simple model are adapted from the Vegetation Photosynthesis Model (VPM[3]):

$$f(T) = \frac{(T - T_{max}) \times (T - T_{min})}{(T - T_{max}) \times (T - T_{min}) - (T - T_{opt})^2} \tag{22}$$

where T_{min}, T_{max}, and T_{opt} indicate minimum, maximum, and optimal temperature for vegetation growth.

The soil moisture (SM) limitation is described as a sigmoid function:

$$f(SM) = \frac{1}{1 + e^{-a \cdot SM + b}} \tag{23}$$

where a and b are both parameters that determine the shape of the function. Soil moisture is calculated from a simple water balance model:

$$SM_t = \begin{cases} SM_{max}, & if\ SM_{t-1} + P_t - E_t > SM_{max} \\ SM_{t-1} + P_t - E_t, & if\ 0 < SM_{t-1} + P_t - E_t < SM_{max} \\ 0, & if\ SM_{t-1} + P_t - E_t < 0 \end{cases} \qquad (24)$$

where SM_{max} is the field capacity of the soil, and P_t and E_t indicate the precipitation and evapotranspiration for month t. We use very simple method to calculate E_t, considering it as a function of total vegetation, temperature, and SM.

$$E_t = k \times NDVI_t \times f(T) \times f(SM) \qquad (25)$$

the coefficient k is an empirical coefficient that convert the right side into the unit of mm/month.

This model is set up to generate NDVI timeseries to test the DLM and overshoot identification, therefore, it is simplified and does not take radiation into consideration. The model is optimized with "SCEoptim" function in the R-package "Hydromat". The optimized model can reasonably well capture the dynamic of NDVI, soil moisture, and evapotranspiration during the 2011 and 2012 drought (Supplementary Fig. 17).

We set up four scenarios to test if overshoot drought can be effectively captured by our algorithm. For Scenario 1, the NDVI is simulated using the observed climate for year 2012. For Scenario 2, spring temperature (February to June) is replaced by the multi-year mean temperature for the corresponding months. For Scenario 3, summer precipitation (May to September) is replaced by the multi-year mean precipitation for the corresponding months. For Scenario 4, summer precipitation is replaced by multi-year mean precipitation plus 30 mm/month, while the model simulated NDVI is replaced by the NDVI simulation from Scenario 1. This is to mimic an NDVI decline due to other types of disturbances instead of drought (e.g., harvest). Based on these modified climate conditions, we also calculated the SPEI values for each scenario using the R package "SPEI" with potential evapotranspiration calculated using the "thornthwaite" method.

Three out of four scenarios show negative anomalies in the summer months, which is essential to be considered as overshoot drought (Supplementary Fig. 18). Based on our definition, Scenario 1 is a typical overshoot drought. For Scenario 2 and 4, no lagged adverse effects contribute to any of the negative anomalies in summer months; for Scenario 3, summer months do not show an evident NDVI decline, therefore, none of these three are considered as overshoot droughts. These represents our prior knowledge.

The DLM decomposes vegetation anomalies into different components, and correctly captures the positive NDVI anomalies induced by spring warming in Scenario 1, 3, and 4, as well as the negative NDVI due to summer precipitation decline in Scenario 1 and 2 (Supplementary

Fig. 19). Out of these two drought events, the lagged adverse effect is only identified at sub-seasonal and seasonal time scales for the Scenario 1, which is consistent with our prior knowledge. For Scenario 2, although the summer drought also induces NDVI decline, it is not attributed to the lagged effect from previous months, and therefore, not considered as overshoot drought. For Scenario 3, although spring warming also greatly stimulates vegetation growth, normal summer precipitation can support this increased water consumption and does not induce NDVI decline. For Scenario 4, the DLM also identifies adverse lagged effect at sub-seasonal and seasonal scales, however, this NDVI anomalies is not induced by drought, and it is not identified as an overshoot drought event.

Supplementary Text 5. Test of spatial autocorrelation

Spatial autocorrelation may potentially affect the correlation calculation between two spatial patterns, and if presents in our analysis could affect the statistical power of the results. To test this effect on our study, we first built a general linear model to model the relationship between the number of overshoot drought events and the number of droughts. If the model performance is affected by a positive spatial autocorrelation, the semivariance (in our case, residual) would increase as a function of increasing distance between observations. If a negative spatial autocorrelation exists, the semivariance would decrease along the distance. This can be tested using a semivariogram (Supplementary Fig. 2). The semivariogram shows that there is no obvious tendency of semivariance along the distance axis, indicating that the spatial autocorrelation has limited effects on the correlation presented in our study.

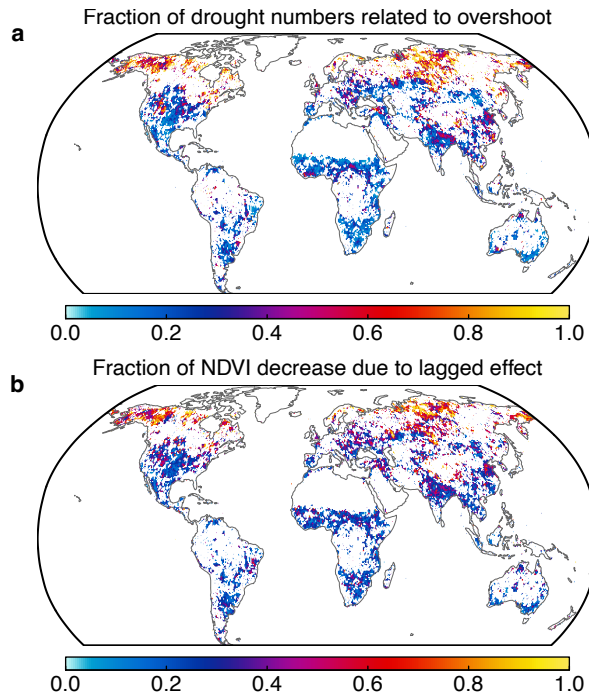**Supplementary Table 1. Additional experiments for the sensitivity analysis.**

	Original model	Reduced model	Extended model	Discrete precipitation model	Exp. 1	Exp. 2	Exp. 3	Exp. 4
Climate variables in DLM	3-month precipitation and temperature	3-month precipitation	3-month precipitation, temperature, and solar radiation	precipitation from current month, previous 1-month, previous 2-month, temperature, and solar radiation				
Minimum drought length	2 months				1 month			
Minimum NDVI anomaly during drought	<−0.1×mean NDVI					<−0.05×mean NDVI		
SPEI threshold for drought identification	-0.5						-1	
Confidential interval for overshoot sensitivity	90%							75%
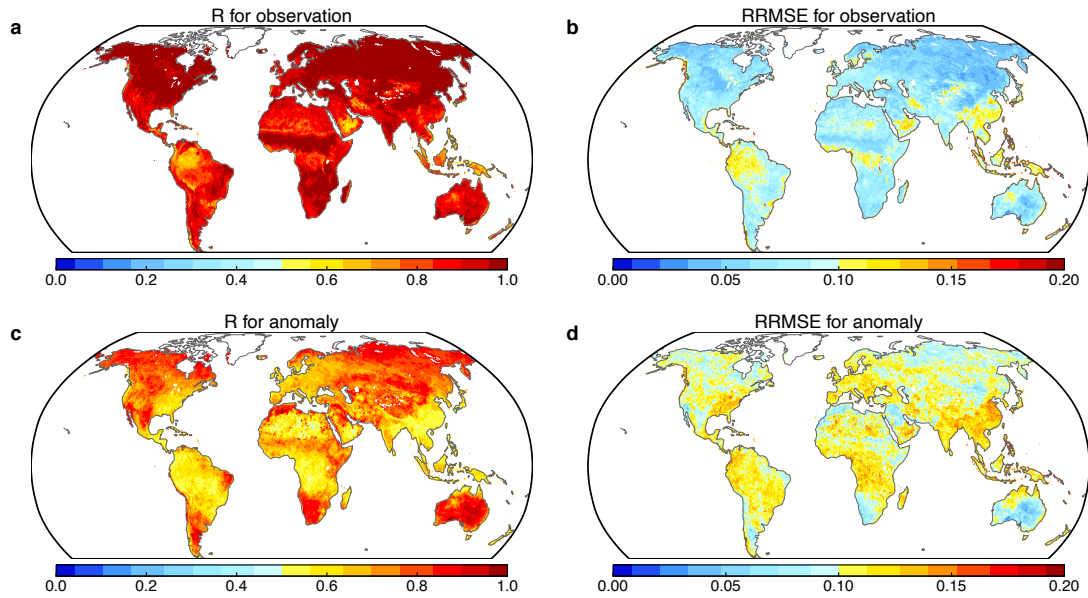
Supplementary Figure 1. Performance metrics for the DLM. Correlation coefficient (**a**) and relative root mean square error (**b**) between satellite retrieved NDVI time series and DLM predicted NDVI. After removing the trend and seasonal component (obtained from DLM) from satellite retrieved NDVI, correlation coefficient (**c**) and RRMSE (**d**) for the observed and DLM predicted de-seasonalized detrended anomalies. The observation of de-seasonalized detrended anomaly is calculated as the raw NDVI time series minus the trend and three seasonal components. The DLM predicted de-seasonalized detrended anomaly is calculated as the summation of precipitation, temperature, and all lagged NDVI components.
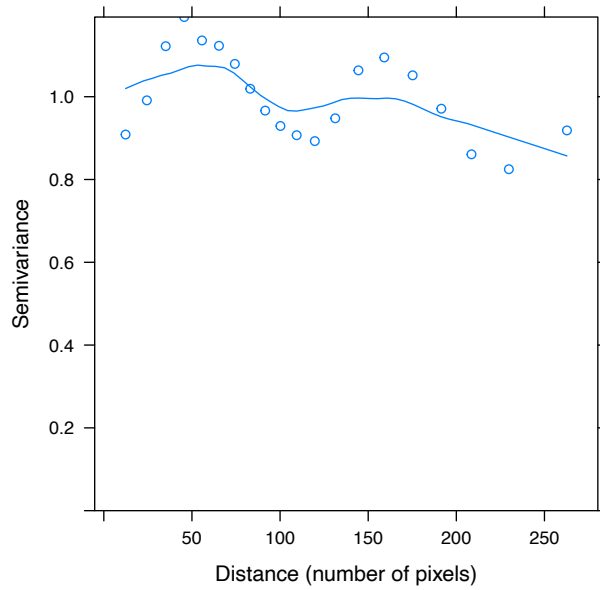
Supplementary Figure 2. A semivariogram showing the relationship between semivariance and distance. The y-axis shows the normalized variance of residuals and the x-axis shows the distance between the observations (in number of pixels). If a positive spatial autocorrelation affects the model performance, that is, the model performs better (low residual) in part because the samples are closer to each other (shorter distance). This will be shown as an increasing trend of semivariance of the residual along the distance axis.

a Fraction of drought numbers related to overshoot

b Fraction of NDVI decrease due to lagged effect

Supplementary Figure 3. Spatial patterns of fractions of overshoot number, impacts for drought events. a Fraction of drought number that are related to overshoot. **b** fraction of NDVI decline during overshoot drought events that are induced by the lagged adverse effect. White regions indicate no overshoot drought detected during our study during 1981-2015.
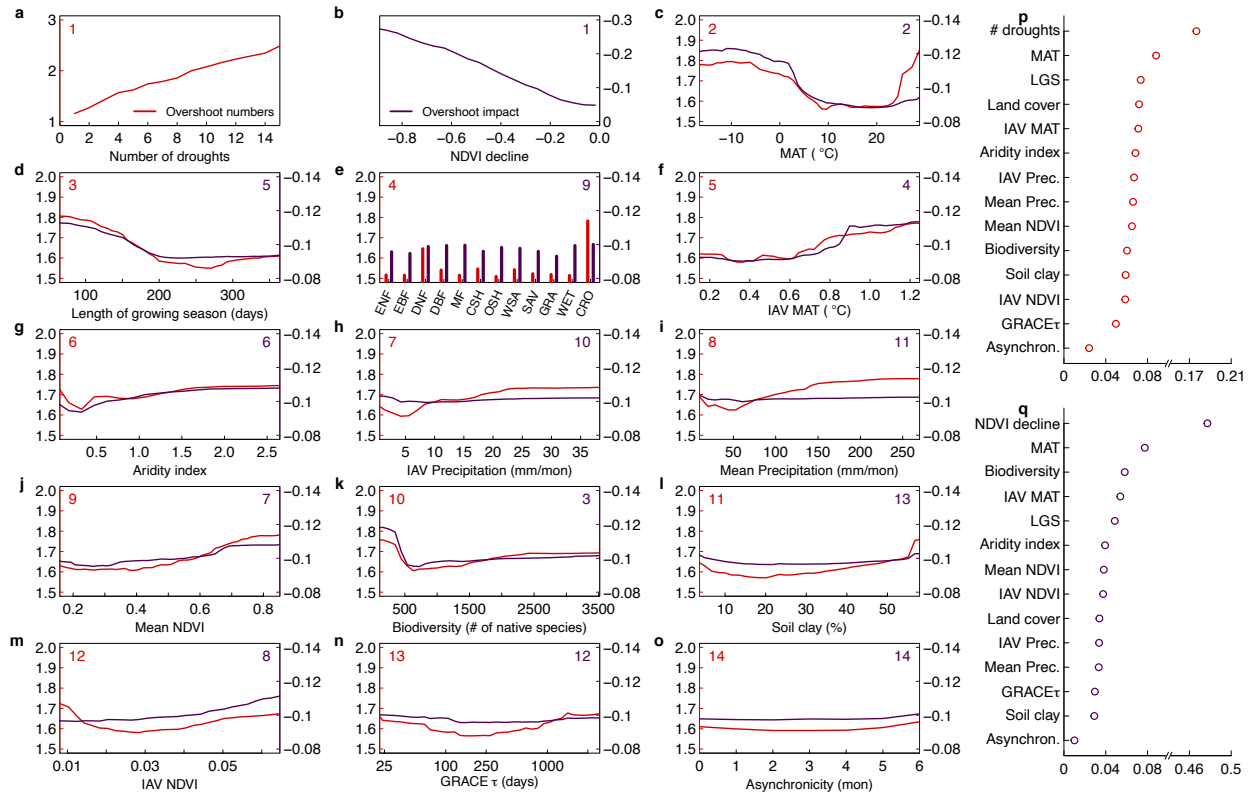
Supplementary Figure 4. Response functions for the predicting overshoot drought number and lagged effects. **a-m**, response functions of number of overshoot droughts, and the adverse lagged effect. The numbers in the top-left and top-right corners indicate the order of importance for predicting the numbers fraction and impacts fraction of overshoot drought, respectively. **p-q** normalized variable importance for predicting numbers (**p**) and lagged effect (**q**) of overshoot drought events.
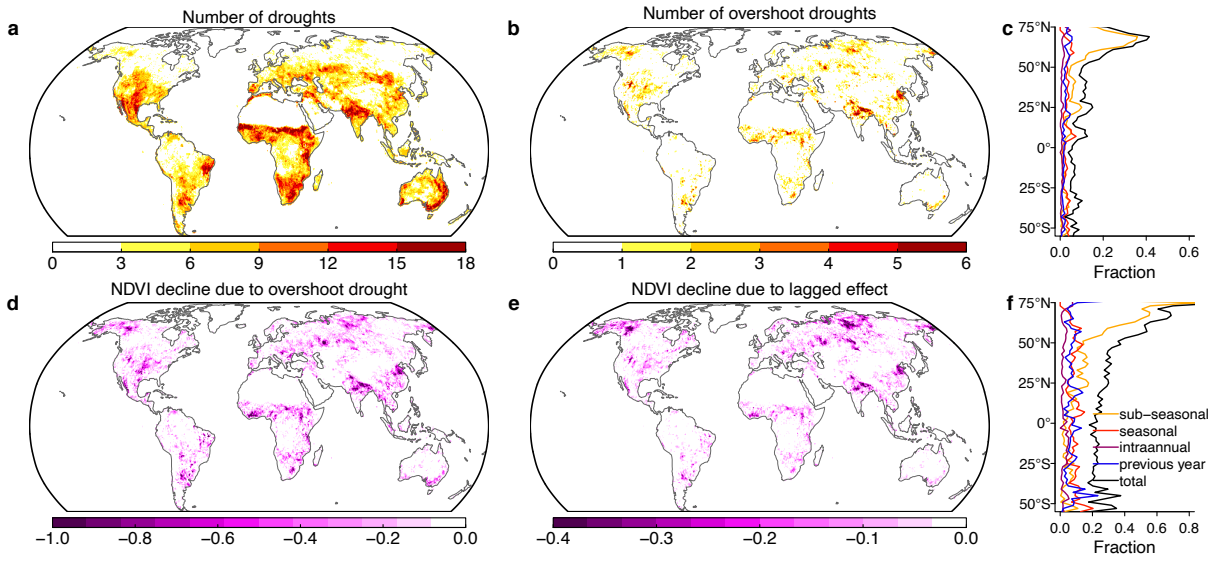
Supplementary Figure 5. Drought and overshoot drought patterns from the "reduced model". Same as Fig. 1, but uses the "reduced model" that does not consider the temperature effect.
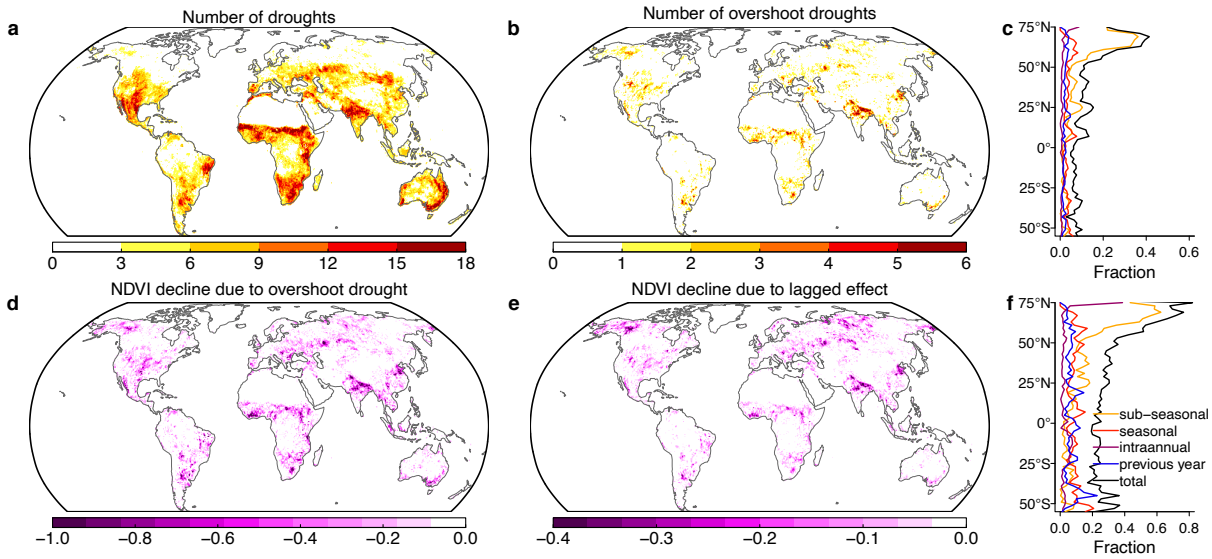
Supplementary Figure 6. Drought and overshoot drought patterns from the "extended model". Same as Fig. 1, but uses the "extended model" that does consider the radiation effect on vegetation.
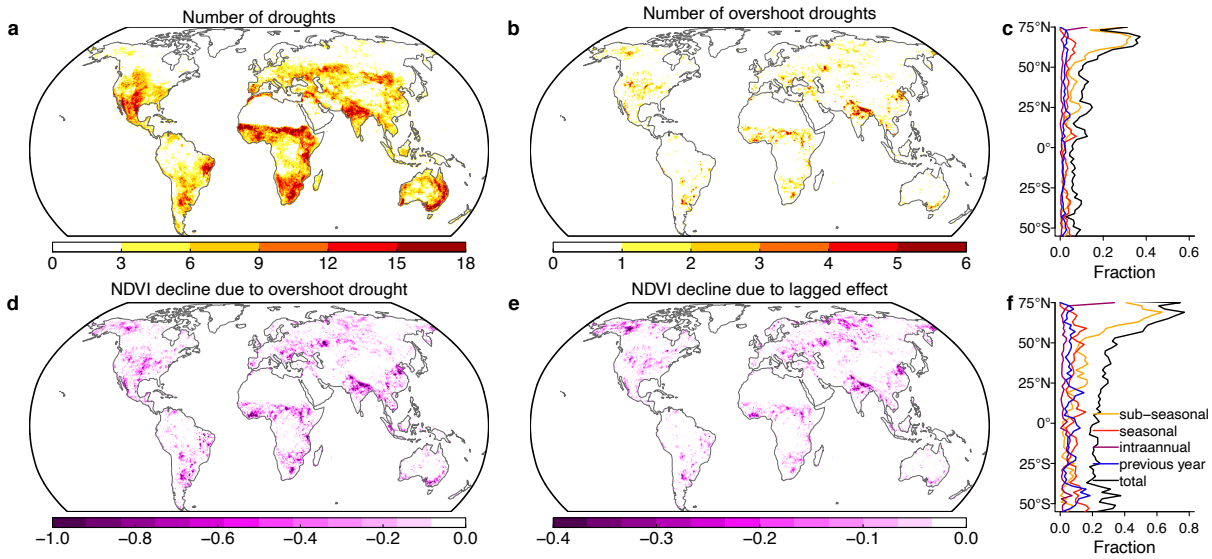
Supplementary Figure 7. Drought and overshoot drought patterns from the "discrete precipitation model". Same as Fig. 1, but uses the "discrete precipitation model" that does consider the climate variables including temperature, radiation, and precipitation from current month and previous 2 months separately.
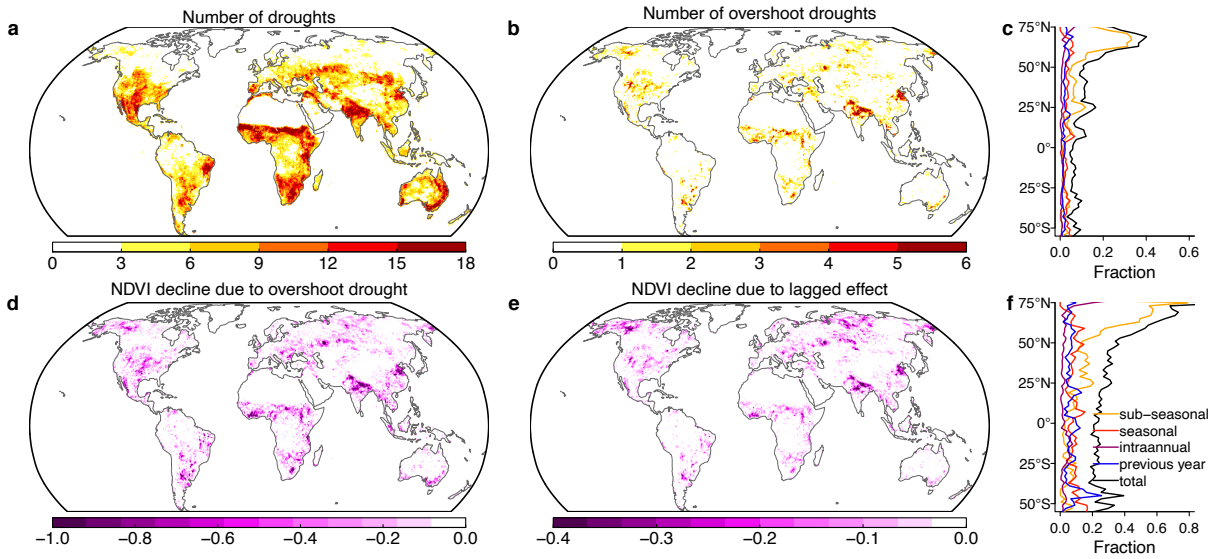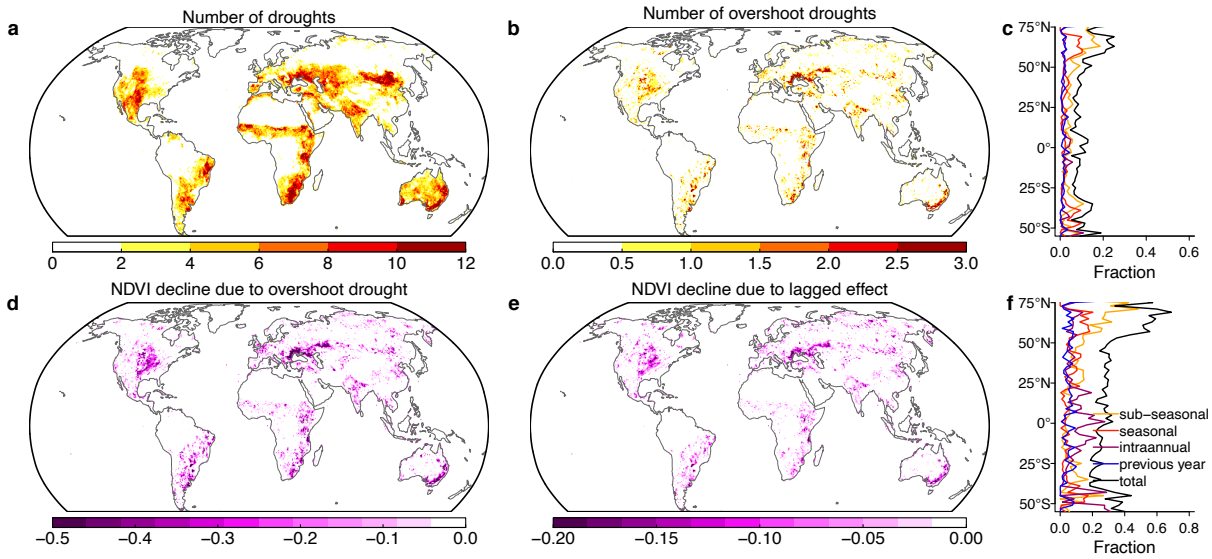
Supplementary Figure 8. Drought and overshoot drought patterns from the Experiment 1.
Same as Fig. 1, but uses the drought length threshold of one month instead of two months. A drought should still have at least consecutive negative NDVI anomalies, however, the second negative value can be greater than 70% of the minimum (first). The drought period is only the first month in this case.
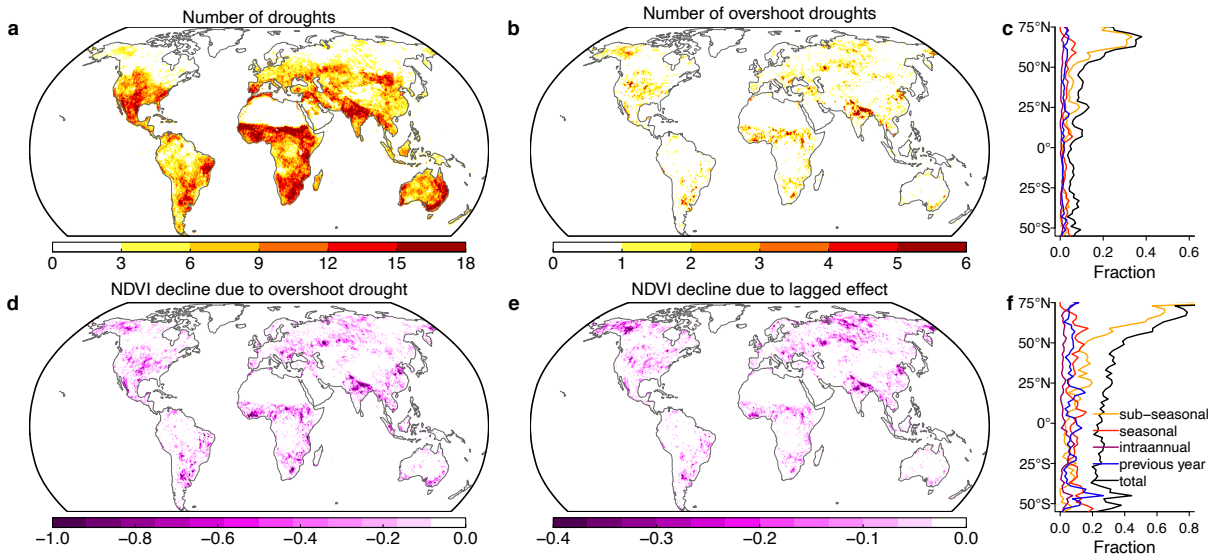
Supplementary Figure 9. Drought and overshoot drought patterns from the Experiment 2.
Same as Fig. 1, but uses a relaxed drought identification threshold. In Fig. 1, the minimum of the de-seasonalized detrended NDVI anomaly during drought should be less (more negative) than -0.1×mean NDVI, while in this experiment, it should be less than -0.05×mean NDVI.
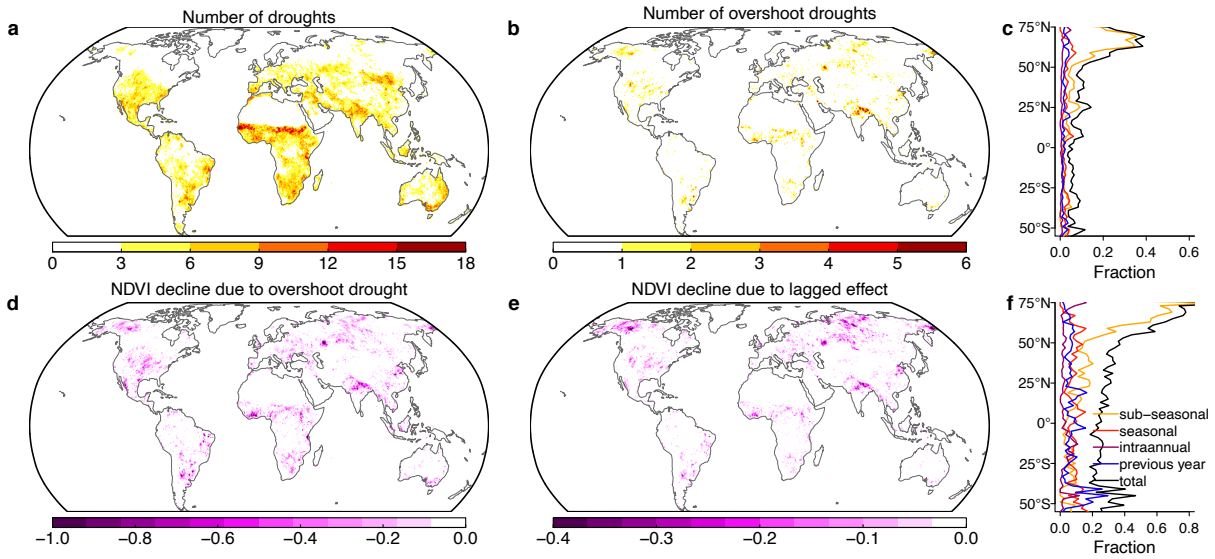
Supplementary Figure 10. Drought and overshoot drought patterns from the Experiment 3.
Same as Fig. 1, but uses a stricter drought identification threshold. In Fig. 1, the mean SPEI during drought should be less (more negative) than -0.5, while in this experiment, it should be less than -1.
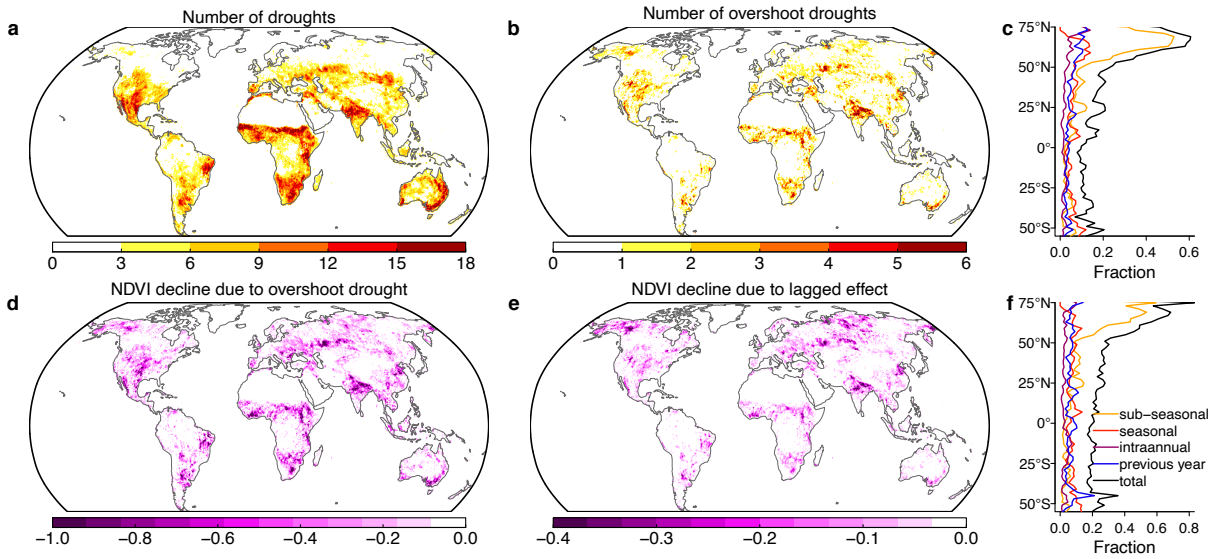
Supplementary Figure 11. Drought and overshoot drought patterns from the Experiment 4.
Same as Fig. 1, but uses the 75% confidence interval of the DLM sensitivity instead of 90% for the overshoot component identification. The DLM sensitivity describes the linkage between previous positive NDVI anomalies and their lagged adverse effect on current NDVI.
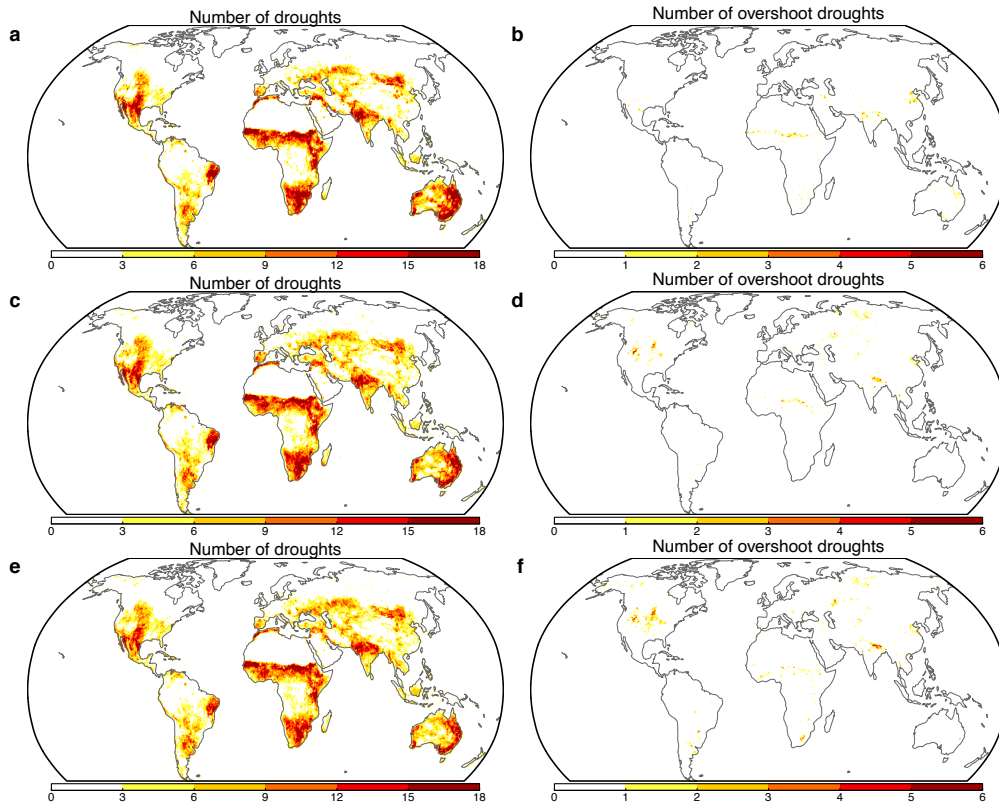
Supplementary Figure 12. Drought and overshoot drought patterns during 2000-2018 based on MODIS NDVI. Same as Fig. 1, but uses MODIS MOD13C2 NDVI. The NDVI data quality is checked using associated VI Quality layer. The DLM recycles observations during 2000-2004 twice as the spin-up period, and uses both precipitation and temperature as the environmental factors.
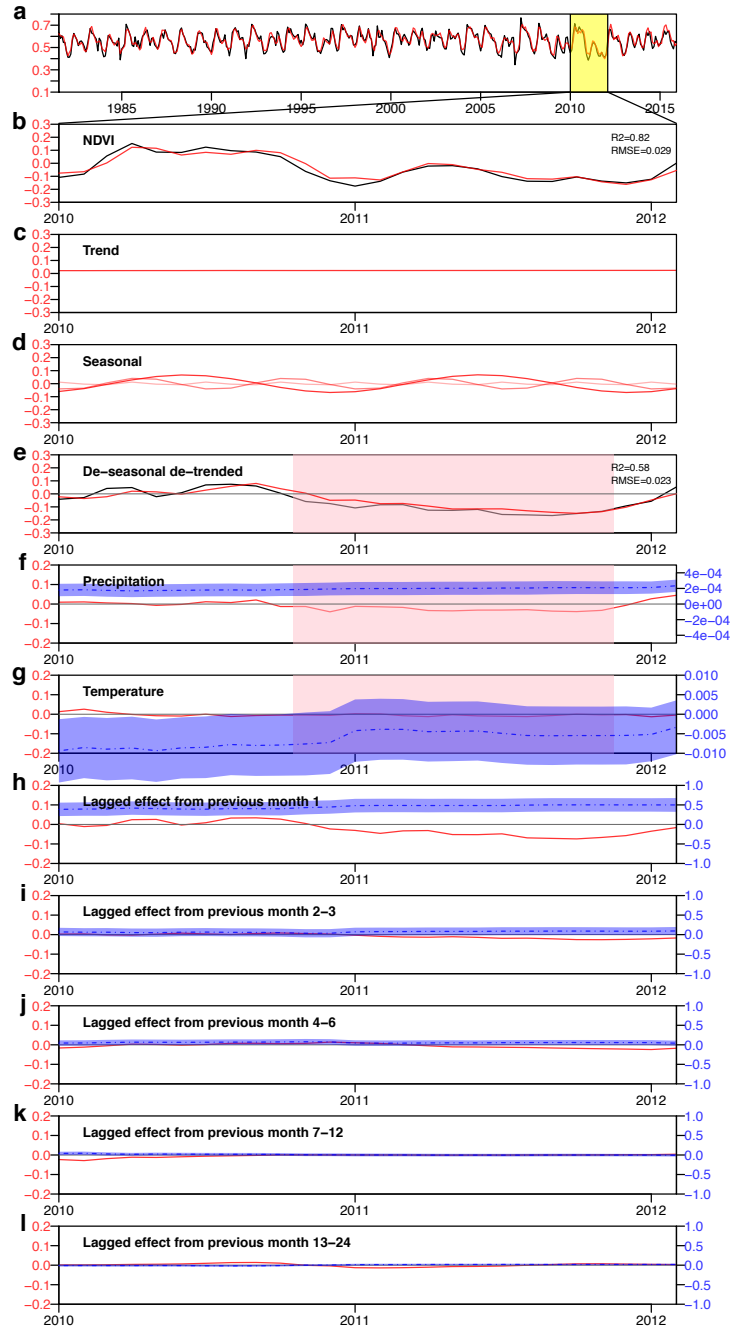
Supplementary Figure 13. An example of DLM decomposition of NDVI time series for one pixel in Texas (Lat=30.76, Lon=-98.93). Same as Extended Data Fig. 2, but for a grassland site in Texas focusing on the 2011 drought. This drought is caused by a long-term water deficit without much lagged effect, thus, not considered as an overshoot drought. The DLM correctly identifies this drought event and does not consider it as overshoot drought.
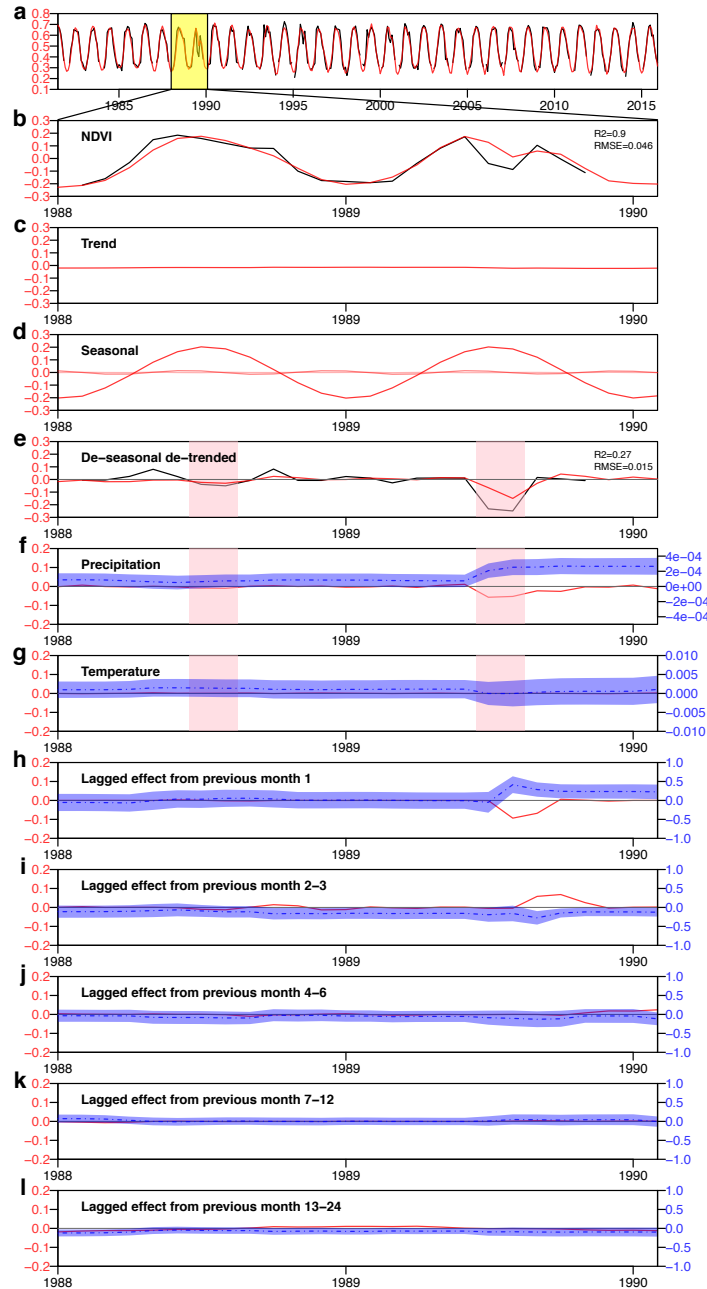
Supplementary Figure 14. An example of the DLM decomposition of one randomized NDVI time series for the same site in Extended Data Fig. 2. The experiment randomly swaps the two consecutive months across years, therefore breaking up the potential linkage of the lagged effect (see Methods and Supplementary Text 3). In this example, the two months of July/August in 2012 were swapped to July/August in 1989, following May/June in 2007 which were swapped to May/June in 1989. Although July and August are still considered as a drought event, they are no longer identified as overshoot drought.

Supplementary Figure 15. Spatial patterns of events number and impact for overshoot related drought events from the randomized experiments. A drought or overshoot drought event is only valid when at least three out of five randomized experiments identify it as a drought or overshoot drought event. **a,b** drought numbers for the randomize experiment with group size of 2 months; **c,d** for group size of 6 months; **e,f** for group size of 24 months.
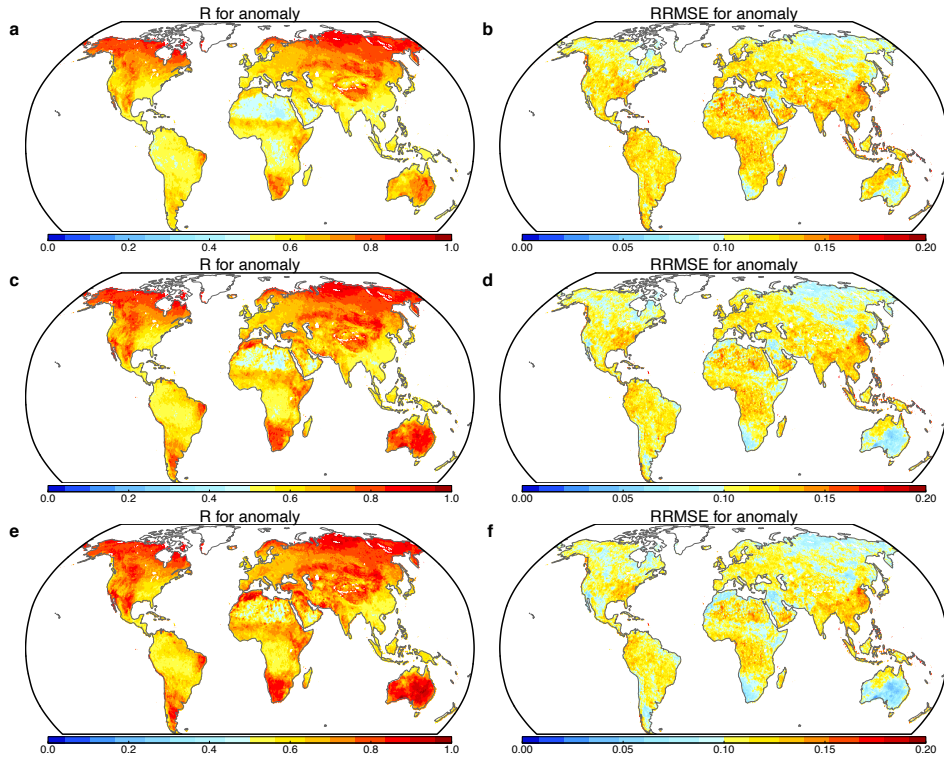
Supplementary Figure 16. Model performance for the randomized DLM. Same as Supplementary Fig. 1c,d, but for the average model performances of five randomized experiments. **a,b** DLM model performance for randomize experiment with group size of 2 months; **c,d** for group size of 6 months; **e,f** for group size of 24 months.
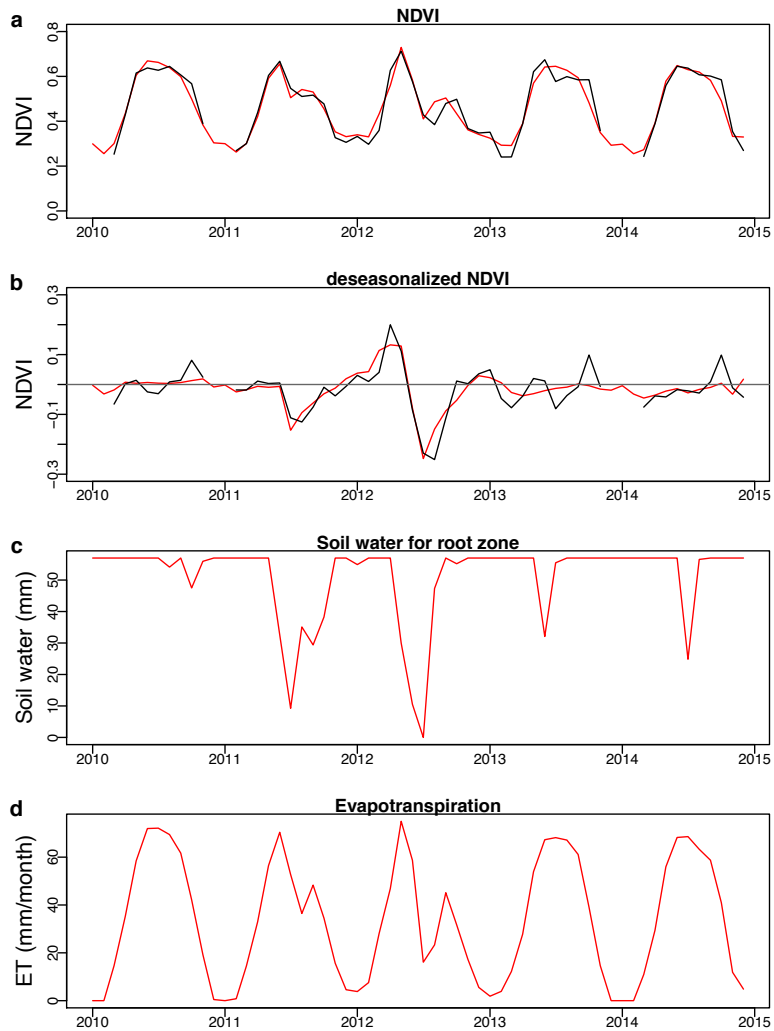
Supplementary Figure 17. Model prediction of NDVI for the Kansas site during 2010-2014 (same as Extended Data Fig. 2). The red lines show the model prediction and the black lines indicate NDVI observation. **a** NDVI, **b** de-seasonalized NDVI anomaly, **c** soil water for the root zone, **d** evapotranspiration.
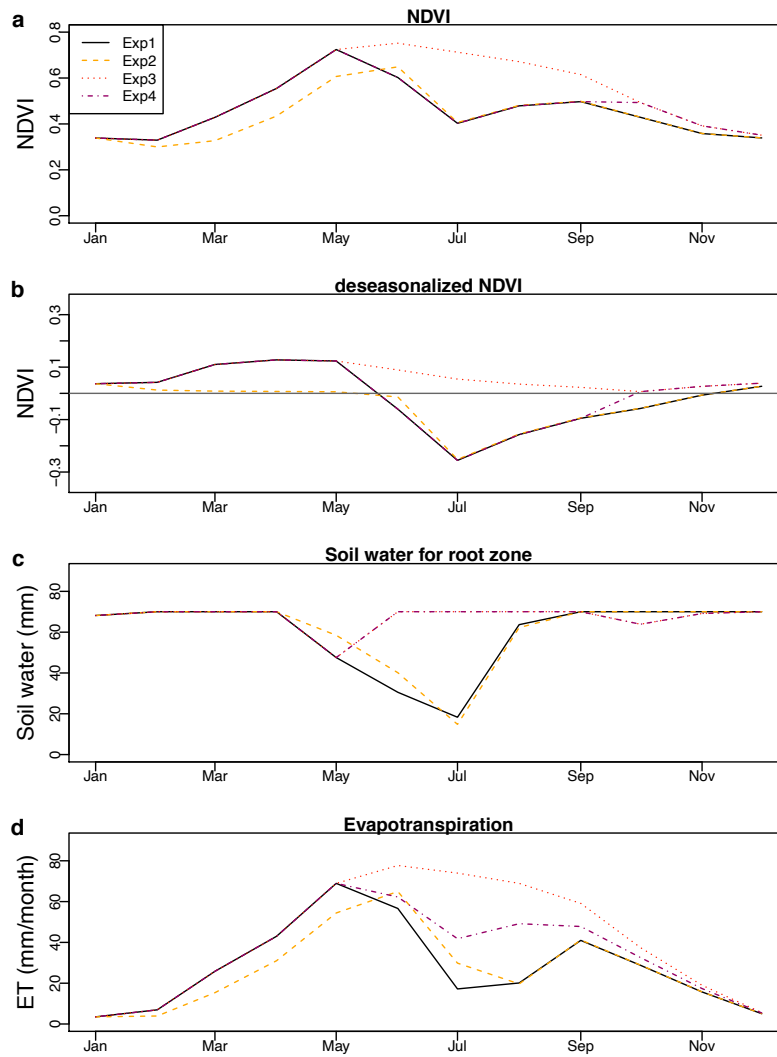
Supplementary Figure 18. Model simulated vegetation and water dynamics for the Kansas site for 2012 drought for the four scenarios. d. **a** NDVI, **b** de-seasonalized NDVI anomaly, **c** soil water for the root zone, **d** evapotranspiration.
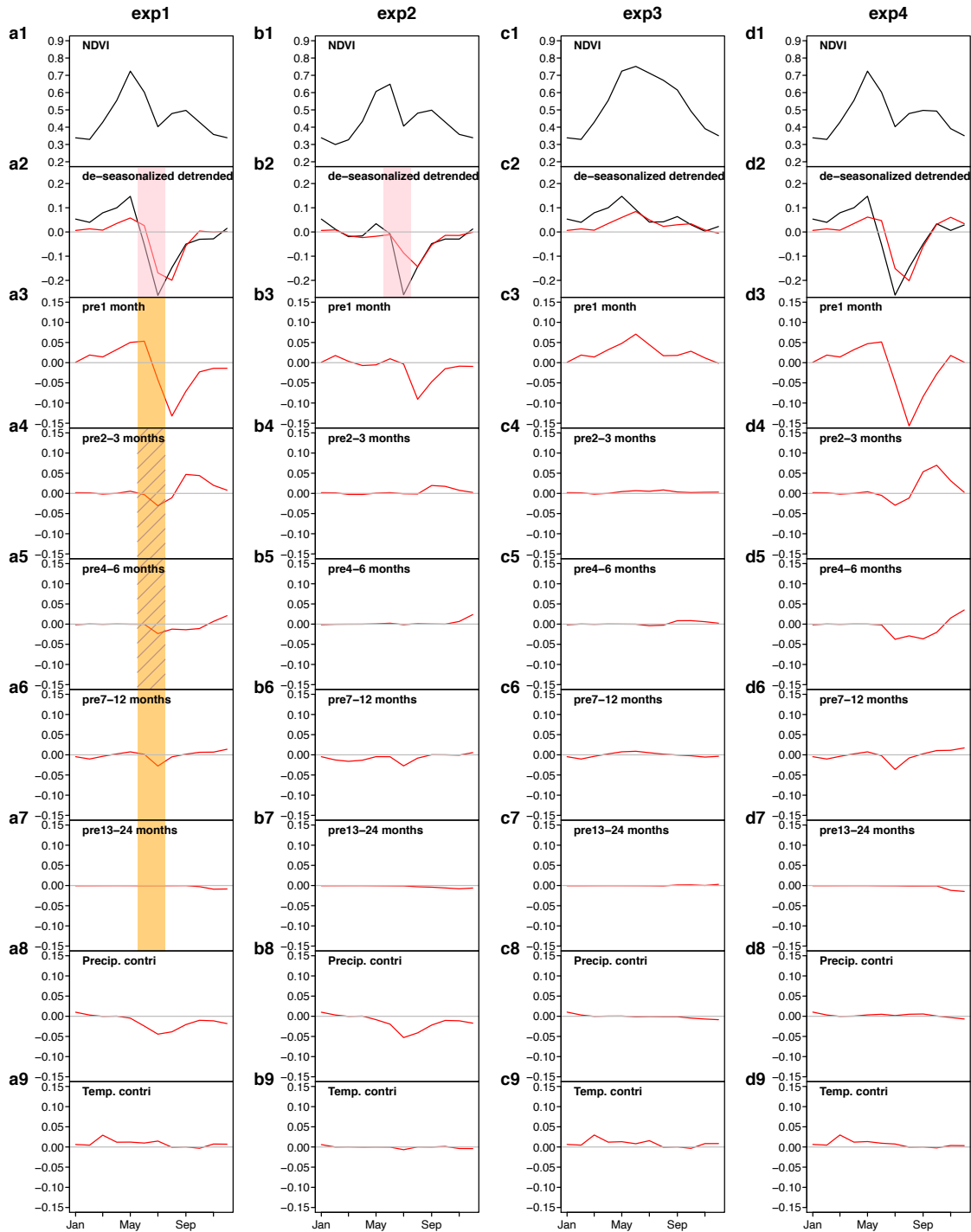
Supplementary Figure 19. Overshoot drought identification for four experiments. a-d each column shows the decomposition of NDVI using the DLM. Black lines in the first two rows are NDVI simulated by the simple model. Red lines are the DLM predictions for each component. Red rectangles in the second row indicate drought events. Orange rectangles in the third to seventh

row indicate the drought is an overshoot drought. Hashed areas in **a4** and **a5** indicate the overshoot component.

References

1. Prado, R. & West, M. *Time series: modeling, computation, and inference*. (CRC Press, 2010).

2. Wolf, S. *et al.* Warm spring reduced carbon cycle impact of the 2012 US summer drought. *Proceedings of the National Academy of Sciences* **113**, 5880–5885 (2016).

3. Zhang, Y. *et al.* A global moderate resolution dataset of gross primary production of vegetation for 2000–2016. *Scientific Data* **4**, 170165 (2017).